Multitemporal ERS SAR Analysis Applied to Forest Mapping

Shaun Quegan, Thuy Le Toan, Jiong Jiong Yu, Florence Ribbes, and Nicolas Floury

***Abstract*—Examination of the physical background underlying the ERS response of forest and analysis of time series of ERS data indicates that the greater temporal stability of forest compared with many other types of land cover presents a means of mapping forest area. The processing chain necessary to make such area estimations involves reconstruction of an optimal estimate of the backscattering coefficient at each pixel using temporal and spatial filtering so that classification rules derived from large scale averaging are applicable. The rationale behind the filtering strategy and the level of averaging needed is explained in terms of the observed multitemporal behavior of forest and nonforest areas. Much of this analysis is generic and applicable to a wide range of situation in which significant information is carried by multitemporal features of the data. The choice of decision rules is based on the forest observations, with the added requirement for robustness. The performance of a classifier based only on change is assessed on a range of test sites in the U.K., Finland, and Poland. Error sources in this classifier are identified, and the possibility of improving performance by including radiometric information in the mapping strategy is discussed. Brief discussions of how the classification is affected by the addition of coherence and how the processing chain would need to be modified for other forms of satellite data are included.**

***Index Terms*—Backscatter modeling, change detection, image classification, image filtering.**

I. Introduction

THE PAST decade has seen the deployment of four satelliteborne Synthetic Aperture Radar (SAR) systems for remote sensing of the Earth's surface: ERS-1 & 2, JERS-1, and RADARSAT. Each of these operates at a single frequency and polarization. Apart from JERS-1, which provided L-band data until October 1998, they are C-band systems that have provided SAR data on a continuous basis since 1991. C-band services, with increased flexibility in terms of incidence angle, resolution, and polarization, will continue well into the millennium with Envisat-ASAR (2000) and Radarsat II (2002). A number of other satellite SAR's are mooted, but multichannel systems comparable to the Shuttle or airborne radars are not an immediate prospect. It is therefore important to exploit the full potential of the available, relatively simple C-band systems.

A major part of this potential stems from the fact that operational and environmental science users are often interested in dynamic processes. Satellite SAR's can reliably provide the multitemporal data needed for observing such processes. Hence, attempts to use multitemporal SAR data in various disciplines have grown significantly, with forest studies being one of the most active areas. Numerous research results indicate that SAR can contribute to mapping vegetation cover in regions characterized by frequent cloud cover (e.g. tropical and boreal forests) and monitoring changes in the forest environment, both man-made (deforestation, clear-cutting) and natural (phenology, freeze/thaw status of vegetation, storm, fire damage, etc.). These are essential pieces of information in studies of forest resources and ecosystems and their contribution to the global carbon cycle.

C-band SAR has received less attention in this context, since most studies have emphasized higher biomass forests, for which C-band systems are unsuited. This is because the backscatter saturates when biomass exceeds a certain level, with higher levels occurring for longer wavelengths. Total biomass of up to 150–200 tons/ha can be retrieved from P-band images, whereas at C-band, saturation occurs at 30–50 tons/ha [1]–[4]. Since forest biomass can exceed 500 tons/ha, C-band displays little sensitivity to spatial or temporal forest variations in many parts of the world. However, low biomass forests are of interest for a variety of reasons.

1) European policies will encourage conversion of land to forestry, with an associated monitoring need.
2) Information on regenerating forests is important in understanding forest dynamics.
3) Low density forests of the sub-Arctic zone should be very sensitive to climate warming.

Moreover, changes in forest cover due to clearcutting and burning mark a drastic change in biomass, whose mapping on a global scale is important.

Despite this, a variety of reasons hinder effective use of the available C band SAR data in forest observations.

1) Single SAR images, especially at C-band, often show little differentiation between forest and other types of vegetation cover.
2) The value of multitemporal data for forest studies has not been widely reported.
3) Results of forest mapping suffer from a lack of quantitative validation.

Manuscript received May 10, 1999; revised November 30, 1999. This work was supported by the EU-funded European Forest Observations using Radar (EUFORA) project [ENV4-CT96-030] and JRC/CEO Contract Forest Monitoring in Europe with Remote Sensing (FMERS-I, Contract BI 05-97-07 F1ED ISP SF).

S. Quegan and J. J. Yu are with the Sheffield Centre for Earth Observation Science, University of Sheffield, Sheffield, U.K (e-mail: s.quegan@sheffield.ac.uk).

T. Le Toan and F. Ribbes are with the Centre d'Etudes Spatiales de la Biosphere (CESBIO), Toulouse, France.

N. Floury is with the European Space Research Centre (ESTEC), Noordwijk, The Netherlands.

Publisher Item Identifier S 0196-2892(00)02092-1.

TABLE I
AVAILABLE MULTITEMPORAL ERS DATA FOR THETFORD, U.K.

Sensor	Year	JAN	FEB	MAR	APR	MAY	JUN	JUL	AUG	SEP	OCT	NOV	DEC
ERS-1	1992					•	•	•	•	•	•		
ERS-1	1993	•	•	•									
ERS-2	1997	•	•	•	•	•	•		•	•	•	•	•

4) Suitable analysis methods and computer software are unavailable to potential users of SAR data for forest information.

This study therefore has two main objectives. The first is to explain the role of multitemporal data in mapping forests. This requires investigation of the physical background to the problem, coupled with data analysis (Section II). Our second objective is to define generic methods of dealing with multitemporal ERS SAR data. We will show in Section III that the properties of this type of data lead to simple and efficient methods with constraints arising naturally from the data analysis. Section IV is concerned with validation of the mapping methods, while Section V summarizes the approach, describes how to generalize it to other SAR data, and briefly discusses its relation to mapping based on interferometric coherence.

II. DATA ANALYSIS AND PHYSICAL PRINCIPLES

A. Data Description

To provide a context for our approach, we first examine multitemporal data from Thetford, U.K., which is a forest site surrounded by a complex pattern of grassland, heath, and fields containing various types of crops. Two separate areas of the forest are considered, namely West Harling and King's Forest, each of which is managed by the U.K. Forestry Commission (UKFC). The region is flat and has a continental climate with one of the lowest rainfalls in the country. The soil is porous, dry, and contains flints, sand, and chalk. Corsican pine is the main timber tree ($> 50\%$), and the remainder of the forest consists of deciduous species (i.e., oak and beech), Scots pine, and other conifers such as larch, fir, etc. Corsican pine is the preferred species because of its superior timber quality and growth rate compared to Scots pine.

The UKFC provided stock maps for West Harling, last updated in 1996, and for King's Forest, updated in July 1997. Digitized maps of West Harling and King's Forest were generated from the two stock maps. These show stand boundaries, species, planting year, and compartment areas, but information about biomass and stem volume was not available. However, biomass normally increases with stand age, except where thinning causes an abrupt decrease. Information about woodland areas outside the managed forest were based on the 1:10,000 Ordnance Survey maps.

The SAR data available for this test site consists of two full-year coverages by ERS PRI images with nine ERS-1 images in 1992/3 and eleven ERS-2 images in 1997 (see Table I).

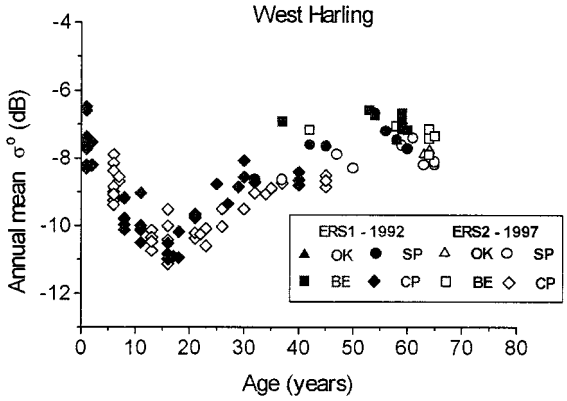

Fig. 1. Backscattering coefficient versus age for forest stands in West Harling.

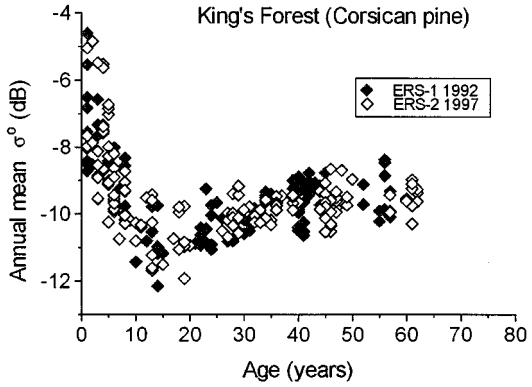

Fig. 2. Backscattering coefficient versus age for forest stands in King's Forest.

These images were all acquired from the 35-day repeat cycle, so they have practically identical geometries.

B. Backscatter Behavior as a Function of Forest Biomass

A plot of average annual backscattering coefficient against age and species for West Harling, using both the 1992/3 and 1997 ERS data sets, is shown as Fig. 1. Each point corresponds to a single stand and stands of Corsican pine (CP), Scots pine (SP), oak (OK), and beech (BE) are included. Note the transition to almost exclusive planting of Corsican pine since 1960. The stands of other species are all at least 37 years old. By contrast, none of the Corsican pine stands is more than 45 years old. A wider range of ages, from 0 to 65 years, is available for Corsican pine in King's Forest, as shown in Fig. 2.

Similar behavior occurs for both years and at both sites. Corsican pine displays a characteristic profile, in which the mean

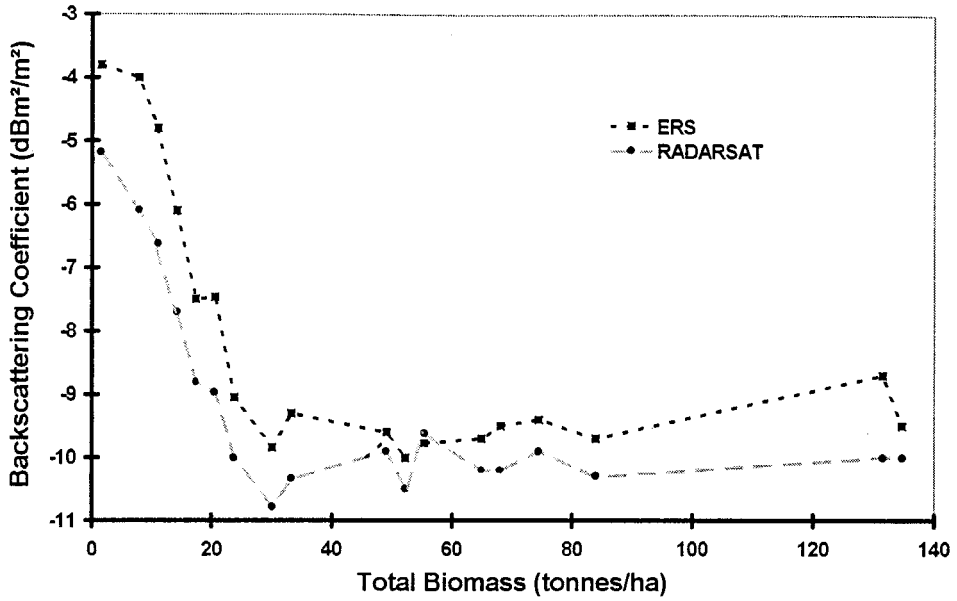

Fig. 3. ERS and Radarsat backscattering coefficient versus total biomass, Landes forest.

backscatter first decreases with age, reaching its lowest level around 15–20 years, then increases to a saturation level around −9 to −10 dB. (A similar profile for Corsican pine at Thetford was observed in airborne AIRSAR C-band data [5]). Different species saturate at different levels. The deciduous species are about 2 dB brighter than the Corsican pine, with a saturation level around −7.5 dB, while Scots pine lies between the Corsican pine and the deciduous species.

Certain general properties of these plots can be readily understood using results from a Radiative Transfer model constructed for the modelling of pine forest [6], [7]. This shows that, for young stands with low biomass, the backscatter at C-band is mainly the sum of direct contributions from the soil, attenuated by the canopy, and the canopy itself. Both the canopy scattering and attenuation come principally from the needles and twigs. The decline in backscatter with age (or biomass or volume) arises from increasing attenuation and is an indication of allometric relations between the total biomass and the biomass of needles and twigs. The backscatter level and the slope of the curves depends strongly on the ground return, which is time and site dependent.

Saturation is readily explained if the canopy is assumed to contain a single category of scatterers with sufficient biomass to reduce the soil contribution to negligible proportions. An elementary calculation then shows the backscattering coefficient to be independent of the number of scatterers, but dependent on their distribution in size, orientation, and dielectric constant [8]. Hence, different saturation levels can arise for different species. Among the coniferous species, maritime pine gives a higher response than Scots pine, which is in turn above Corsican pine, in accordance with the diameters of their needles. Deciduous species generally have higher backscatter than coniferous species, but more work needs to be done to assess the effect of the shape of the scatterers (leaves), as well as the relative importance of attenuation and scattering. Note that stands can vary by about 2 dB for a given stand age. This may arise from the use of

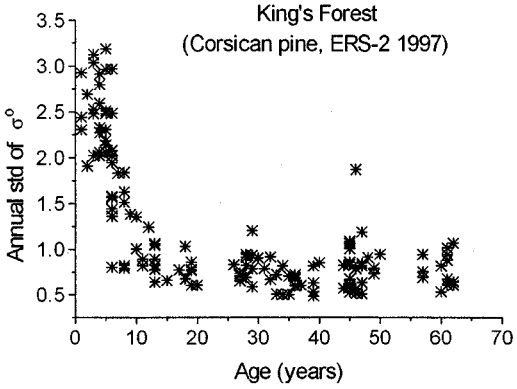

Fig. 4. Annual standard deviation of backscatter versus age for King's Forest.

age instead of biomass to characterize the younger stands, but could indicate structural differences in the saturation zone.

While the initial decline and the long term saturation are general properties, the intermediate behavior may depend on the particular site. This is illustrated by Fig. 3, which plots backscatter against above-ground biomass for the Landes forest, France, using ERS data on December 15, 1996 and Radarsat (at 23° incidence angle) on December 25, 1996. Each data point is the average backscattering coefficient within a stand of 20 to 25 ha. The small difference between ERS and Radarsat may be due to imperfect calibration, the effect of polarization (ERS operates at VV, while Radarsat is an HH system), and changes between the two dates. Unlike at Thetford, there is no significant dip separating the initial decrease in backscatter from the saturation region (which here occurs when biomass reaches 30–50 tons/ha, corresponding at the Landes to 10–15 years). This is likely to represent a different balance between the roles of attenuation and canopy scattering at the two sites, but quantitative confirmation of this would require detailed ground measurements from Thetford. Interpretation is complicated by the fact that thinning is carried out at Thetford

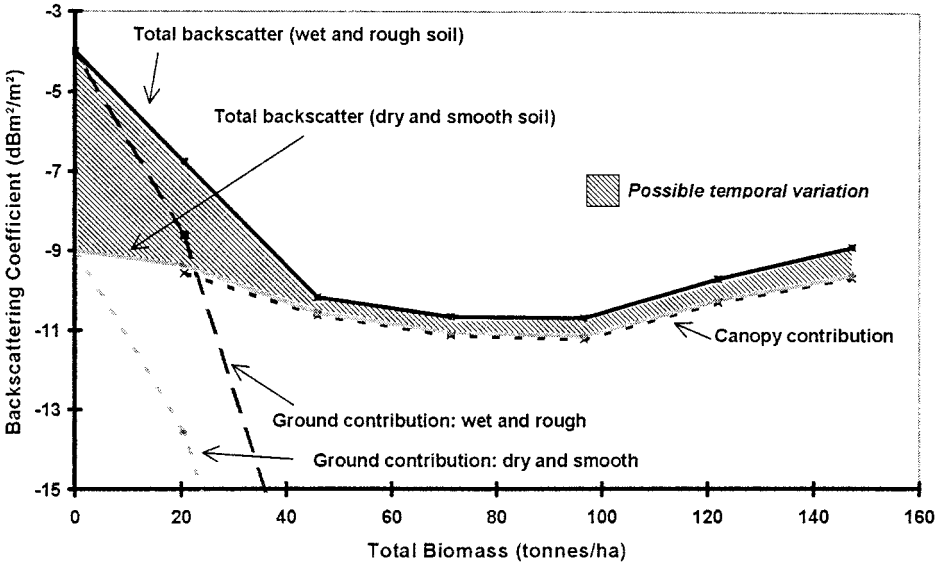

Fig. 5. Simulated backscatter as a function of total biomass for different soil conditions, Landes forest.

when the stands reach the age of 15–20 years, coinciding with the dip in the response.

Even at Thetford, differences can occur due to particular forestry practices. For example, Figs. 1 and 2 show that the clearcut and very young forest areas in King's Forest exhibit higher backscatter than at West Harling. This is thought to be due to the practice of piling forest cutting remnants into long ridges at King's Forest, making the ground surface effectively rougher.

C. Temporal Variation of SAR Intensity in Forest and Nonforest Areas

Temporal variability also exhibits a characteristic dependence on age or biomass. This is clear in Fig. 4, which displays the annual standard deviation in backscattering coefficient plotted against age for 1997 ERS-2 King's Forest data. An initial sharp decrease is followed by variation of around 0.5 to 1 dB for all stands older than ten years (with a currently unexplained outlier at 47 years).

Simulations of the C-band VV backscattering coefficients at 23° incidence using the model decribed in [6], [7] provide significant insight into this behavior. Fig. 5 shows calculations for two different soil conditions: wet and rough and drier and smoother, as biomass is increased in steps of 20 tons/ha. The former conditions correspond to those observed at the Landes forest at the ERS date in Fig. 3, with a volumetric soil moisture content of about 30% and surface rms height of 1.8 cm, while the values in the latter case are 15% and 1.2 cm, respectively. Fig. 5 also decomposes the total backscatter into a ground contribution that changes with soil conditions, and a canopy contribution that remains stable. The dashed area indicates the range of possible temporal change brought about by soil moisture changes. These mainly affect the lowest biomass range, where the behavior can change from a marked decrease with biomass when the soil is rough and wet to a slight decrease under dry conditions.

The temporal behavior of nonforest areas is usually different, both qualitatively and quantitatively. A given change in soil moisture causes greater variation in clear-cut areas or bare soil surfaces than in forest. Agricultural fields display marked changes due to soil moisture, surface roughness, and vegetation growth. Water bodies exhibit large, irregular changes due to the effects of wind. Grasslands and urban areas are stable, but with backscattering coefficients that are lower than forest for grasslands and higher for urban areas.

These differing behaviors are illustrated for a selection of forest and nonforest samples in Fig. 6. For the forest, each plotted point represents a Corsican pine stand of a given age, selected from the data used to form Fig. 2. The nonforest samples are taken randomly from the surrounding agricultural fields, which in this region are likely to contain cereals, sugar-beet, oil-seed rape, and grassland (but no detailed information is available). Observations from a given sample are joined by lines to aid interpretation.

The older forest stands, shown in Fig. 6(a), exhibit little variation through the year, but two populations can be distinguished by their backscatter level. The four highest curves are from 47–60 year old stands, so that saturation in the range −10 to −8 dB has occurred. The lowest three curves, lying between −10 and −13 dB, come from 13–15 year old stands which are therefore near the bottom of the dip in Figs. 2 and 3. Young stands are shown in Fig. 6(b) and tend to exhibit higher backscatter and larger variability, as expected from Figs. 2 and 4. Most of the nonforest areas shown in Fig. 6(c) have backscatter values lying well outside the forest range at some times in the year but, at any one time, forest and nonforest may appear similar. However, the latter exhibit more varied temporal change, corresponding to the variety of vegetation covers in this region. For example, cereals would be expected to have a backscattering coefficient of −5 to −10 dB in winter, falling to −15 to −20 dB in early summer, before increasing again in autumn, whereas oil-seed rape is more stable, with a dip in spring [8], [9]. Sugarbeet has high variability in winter to spring, then stabilizes in summer, while grassland is stable throughout the year.

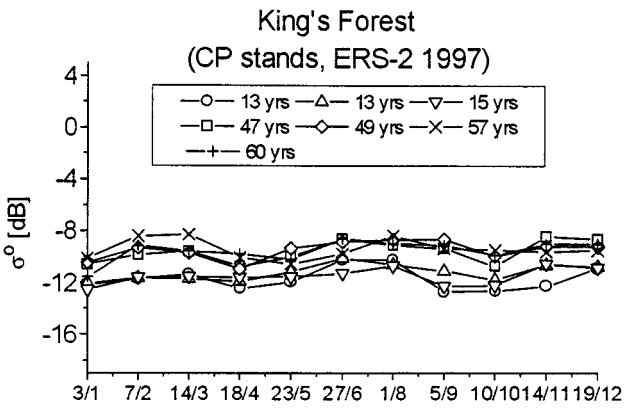

(a)

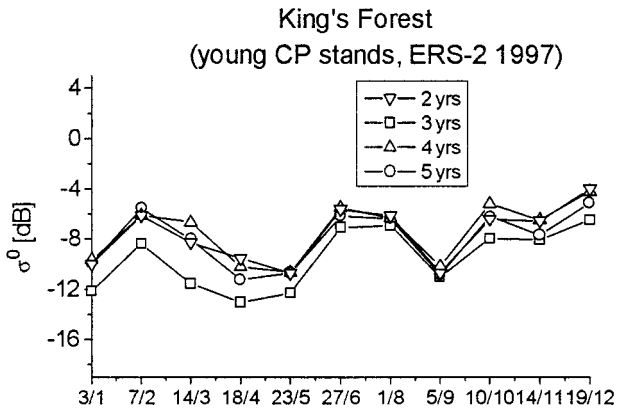

(b)

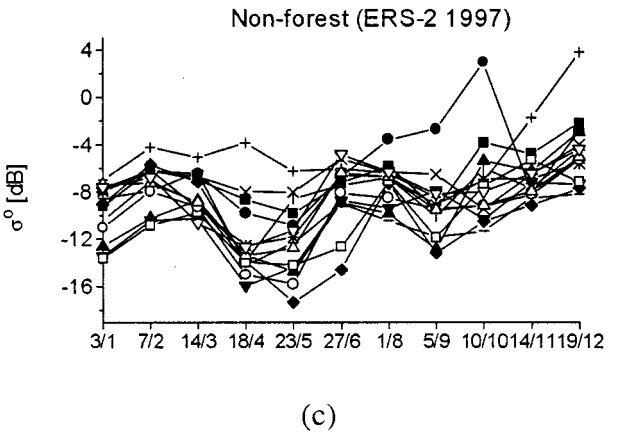

(c)

Fig. 6. Temporal curves for King's Forest area: (a) old forest, (b) young forest, and (c) surrounding nonforest areas.

In addition, the nonforest areas tend to have much greater temporal variability. This is clear from Fig. 7, which shows the maximum change throughout the year of the forest stands in Fig. 6(a) and (b), arranged in order of increasing age, and a larger sample of nonforest areas. Young forest exhibits changes up to 7 dB, but this drops to 2.5 dB for the older forest. Every nonforest region changes by at least 5 dB. Hence, temporal stability provides a possible characteristic by which older forest can be discriminated from nonforest areas.

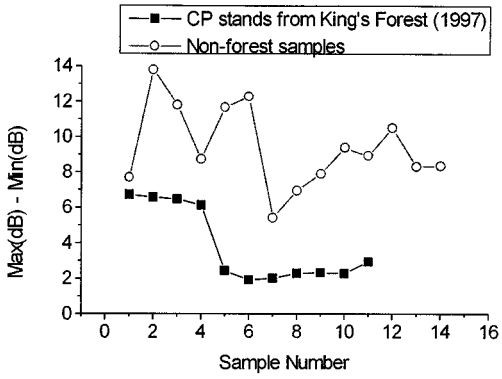

Fig. 7. Maximum intra-annual backscatter change of forest and nonforest samples. Forest samples 1–4 are from forest stands less than six years old.

The effects of weather can be observed in each of Fig. 6(a)–(c) but are more significant for young forest and nonforest areas. The lower values in January present in all three plots correspond to the only date with frost and snow. For the more extreme conditions occurring in boreal forest, frost has been observed to reduce the backscatter and increase the annual variability of older forest [10]. This effect appears to be marginal for the more temperate conditions occurring in Thetford, probably because the frost is not severe enough to modify the vegetation dielectric constant. The June increase in backscatter observed for many of the areas in Fig. 6(b) and (c) occurred during a rainy period and is probably due to increased soil moisture in combination with cereal crop development.

In summary, the C-band backscattering coefficient of forest is stable for stands above 30-40 tons/ha and exhibits higher variability for younger stands mainly due to changes in soil moisture. Without prior knowledge of an area, the temporal variation of C-band intensity data can be used to distinguish the following two general classes:

- vegetation cover exceeding 30 tons/ha, which we interpret as older forest;
- vegetation cover less than 30 tons/ha, which we consider as nonforest, but which on physical grounds *must include young and sparse forest*.

A known exception is dense grassland with continuously high moisture content, as is common in the U.K. Despite having typical biomass values of only around 4 tons/ha, this type of land cover tends to have a very stable response throughout the year.

When we know that the area of interest consists of forest, two classes can be discriminated. At Thetford, Figs. 4 and 7 (noting that the young forests in the latter figure are at most six years old) suggest that forest less than six to eight years should be distinguishable from older forest. At the Landes, the availability of detailed ground data allows this boundary to be expressed in terms of biomass, with a separation between the two classes at around 30 tons/ha. Such prior knowledge that

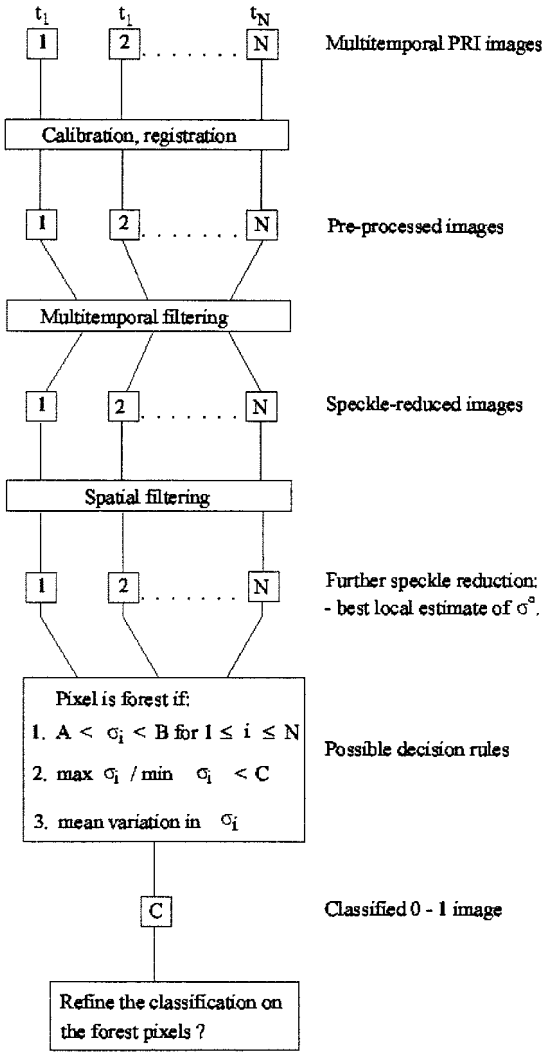

Fig. 8. Processing strategy for forest/nonforest mapping using multitemporal ERS PRI 35-day repeat data.

an area is forest may be available, for example, either because of planned conversion of land to forestry or when the scene is dominated by forest and water or clearcut areas or particular crops.

III. Forest Mapping Algorithm

A processing strategy for forest/nonforest discrimination has been developed based on the above results, as illustrated in Fig. 8. The procedure assumes that N images from the same 35-day repeat cycle are available and consists of three stages: preprocessing, speckle reduction, and classification. The approach can be considered generic to many applications of multitemporal data, but we here wish to stress how the analysis set out in Section II, and the particular properties of ERS data provide very strong constraints on how the various steps are carried out.

A. Preprocessing

Preprocessing consists of two steps. The first is derivation of σ^0 from the digital number at each pixel, following the procedure in [11]. This ensures that values of σ^0 from different times and in different parts of the image are comparable. The second is registration of the images in the multitemporal sequence. For ERS PRI 35-day repeat data, this requires only image translation (here carried out using autocorrelation methods on urban areas within the ERS frame).

B. Speckle Filtering

The second, critical stage in the processing chain is to estimate σ^0 in each of the N images with sufficient accuracy to decide whether the multitemporal behavior at a given pixel corresponds to forest or nonforest. From Section II, we see that this requires us to distinguish forest areas changing by less than 2 to 2.5 dB from nonforest regions, where the change exceeds 5 dB. Separation of these two classes by thresholding requires data with an equivalent number of looks (ENL) well in excess of 100, if unacceptably high false alarm rates are to be avoided [12], [13].

A major advantage of multitemporal data is that both temporal and spatial filtering can be employed in order to achieve the required ENL. For a sequence of N registered multitemporal PRI images, with intensity at position (x, y) in image k denoted by $I_k(x, y)$, the basic problem in temporal filtering is how to combine them linearly in order to produce N output images $J_k(x, y)$ meeting the following two conditions.

1) J_k is unbiased (i.e., $\langle J_k \rangle = \langle I_k \rangle$ where $\langle \cdot \rangle$ denotes expected value, so that the filtering does not distort the σ^0 values).
2) J_k has minimum variance, so that speckle is minimized.

A Lagrange multiplier method applied to this problem leads to the solution [14], [15]

$$J_k = \sum_{i=1}^{N} A_{ki} I_i \qquad 1 \le k \le N \tag{1}$$

where the weighting coefficients A_{ki} are defined by

$$A_k^t = \langle I_k \rangle \frac{C_1^{-1}\sigma}{\sigma \cdot C_1^{-1}\sigma}. \tag{2}$$

Here, $A_k = (A_{k1}, \cdots, A_{kN})$ is the row vector of coefficients appropriate for output image k, ^{t} denotes transpose, σ is the column vector of mean intensities with transpose given by $\sigma^t = (\langle I_1 \rangle, \cdots, \langle I_M \rangle)$, and $C_I(i, j) = \langle I_i I_j \rangle - \langle I_i \rangle \langle I_j \rangle$ is the covariance matrix of the intensity data. J_k, I_k, $\langle I_k \rangle$, and C_I are all calculated at the position (x, y). The explicit formula (2) for calculating A_k is derived in implicit form in [14].

This general treatment (2) needs estimates of the correlations between the temporal images. However, over the 35-day repeat period, the C-band correlation would be expected to fall to very low values in the type of temperate region considered here, except for areas of undisturbed bare soil and urban areas. Examination of the ERS data and sampling statistics indicates that *measured* correlations can depart significantly from zero as a result of sampling error and significant bias when edges occur in the sampling window. The measured correlations therefore introduce spurious effects into the filtering, and it is more cor-

rect to set them to zero. This leads to a much simplified form of the filter, given by

$$J_k(x,y) = \frac{\langle I_k \rangle}{N} \sum_{i=1}^{N} \frac{I_i(x,y)}{\langle I_i \rangle}, \qquad 1 \le k \le N. \tag{3}$$

Two remarks on the performance of this filter are relevant. Firstly, in principle the temporal filter should not degrade the spatial resolution. In fact, the estimate of the $\langle I_i \rangle$ needed in (3) requires spatial averaging within a window in each image of the temporal sequence. This inevitably leads to some loss of resolution, which is minimized by using an adaptive processing window as described in [16]. However, the adaptivity prevents any simple quantification of the spatial resolution after filtering, since it can vary with position in the image. Secondly, if there are N uncorrelated multitemporal images, each consisting of L-look data, then the filtered data will ideally have $N \times L$ looks. In practice, errors in the estimates of the $\langle I_i \rangle$ reduce this value. For example, temporal filtering of the 11 ERS-2 PRI images from 1997, each of which is three-look, leads to data with approximately 25 looks.

Even with large numbers of images available, the gain in radiometric resolution from temporal filtering alone clearly cannot meet the requirements discussed in Section II. Further gains can only come from spatial filtering, using a strategy that again follows from the properties of the ERS data. In particular, there is little or no detectable texture at the scale of typical processing windows at the resolution and incidence angle of ERS. Hence, the appropriate model for the data is the multilook gamma distribution [13]. For spatially uncorrelated pixels, this would imply that the maximum likelihood estimate (MLE) of $\langle I_i \rangle$ for each image is simply the average of the (intensity) pixels in the window. However, both the sampling of the PRI data and the temporal filtering lead to spatial correlation. While the local average is then no longer the MLE, it still provides an unbiased estimate that we adopt in our processing, again using spatially adaptive methods to preserve resolution. As for temporal filtering, the ensuing spatial resolution will vary with position, and therefore, it cannot be readily quantified at the end of the filtering process. A more sophisticated approach would require estimates of the local spatial correlation at the expense of greatly increased processing time and estimation error, for little probable gain in performance.

Unlike temporal filtering, the maximum possible gain in ENL using spatial filtering is not well-defined, being limited only by the number of pixels available within a typical uniform region in the scene. Hence the processing window can be as large as a typical uniform target. However, larger windows place greater reliance on the effectiveness of the spatial adaptivity and it is safer to choose window sizes defined by the necessary ENL. The analysis in this paper uses windows of size 11×11 pixels. For uniform targets, after allowance for spatial correlation, the temporal and spatial filtering would then together yield an ENL of around 500. Estimation error, spatial adaptivity, and image structure all cause significant reductions in this value and make the ENL spatially variable within the final images. However, the filtering strategy has sufficient safety margin to ensure that the ENL needed for our problem is achieved.

Note that other multitemporal studies have used spatial filtering based on maximum *a posteriori* (MAP) filtering [16], [17], assuming gamma distributed texture. Because this is not the appropriate model for ERS data at the scales of interest, the filter tends to leave noise in the output, especially near edges. The images hence appear sharper but need further filtering to reduce classification error [17].

To summarize, the properties of ERS data mean that for this application, only the simplest filtering operations are needed. The complicated part of the filtering strategy is embedded in the spatial adaptivity. Temporal filtering provides an initial improvement in ENL possible for any registered image sequence. Further increases in ENL come from spatial filtering of each image, using window sizes dictated by the problem. Similar conclusions are likely in many other land applications of ERS PRI data, such as hydrology or agriculture.

C. Classification Based on Change

The filtering provides N images, in which each pixel is an unbiased estimate of σ^o, and the ENL has been increased sufficiently to allow reliable decisions to be made on the temporal sequence at each pixel. Forest/nonforest classifications can then be obtained by applying different thresholds to a pixel-based change measure. Three ways of measuring change were considered: annual standard deviation of backscatter, maximum dB difference between any two dates over the year, and mean annual variation (mva). For N images, this latter measure is defined by [18]

$$\text{mva} = 10 \log \left[\frac{2}{N(N-1)} \sum_{i=1}^{N-1} \sum_{j>i} R_{ij} \right] \tag{4}$$

where $R_{ij} = \max(I_i/I_j, I_j/I_i)$ is the normalized ratio of intensities in image i and image j.

Scatterplots and regression lines of one measure against another are shown in Fig. 9, using forest and nonforest 1997 data from King's Forest. The high correlation coefficients imply that at this site, all three measures give equivalent outputs. In general, however, mva and maximum difference measures are to be preferred, since they rely on intensity ratios and hence, are resistant to radiometric distortions caused by topography and systematic calibration errors.

Fig. 10(a) shows mva images based on ERS-1 1992/3 and ERS-2 1997 data for West Harling, and the results of applying thresholds of 2 and 2.5 dB to these images are illustrated in Fig. 10(b) and (c). As expected from the high correlations indicated in Fig. 9, the corresponding maximum dB difference images are very similar and are not shown here. The stock maps are used to indicate the compartment boundaries, and pixels exhibiting change below the threshold are classified as forest. Combining Fig. 7 with Fig. 9(b) suggests a threshold on mva of 2.5 dB to classify the 1997 data (accepting the errors for young forest), but this produces significant misclassification of the nonforest area in 1992/3. Comparisons of the 1992/3 and 1997 data for a sample of nonforest areas in fact indicated much lower values of mva at the earlier date. The reason for this is unknown (for example, rainfall patterns in the two years are not significantly different). Lowering the threshold to 2 dB reduces

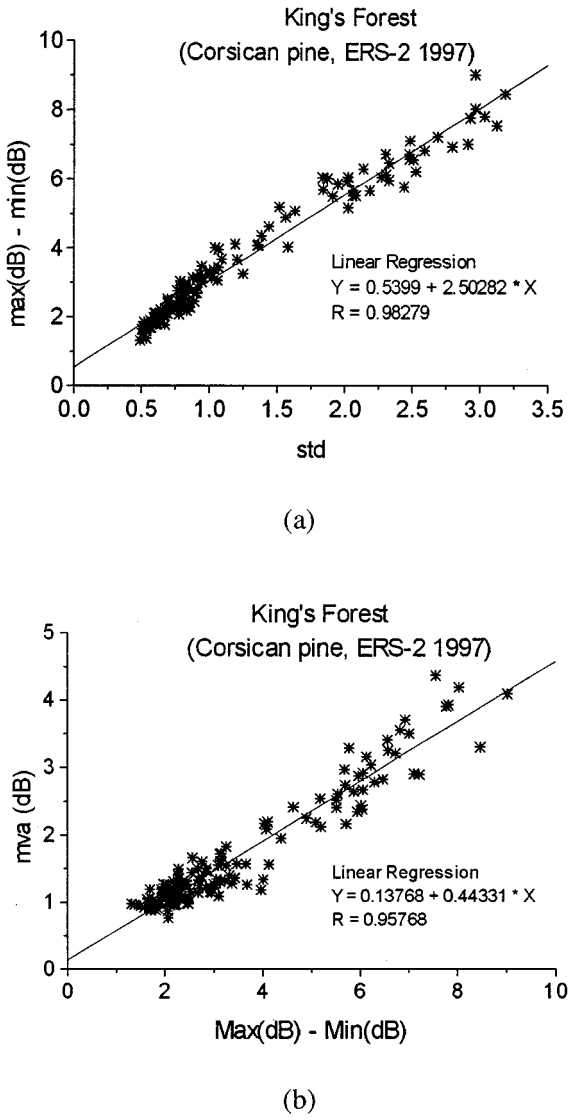

Fig. 9. (a) Maximum dB difference versus std and (b) mva versus maximum dB difference.

the misclassified area outside the forest in 1992 but leads to increased misclassification of young forest in 1997. If an unsupervized common threshold is desired, 2 dB seems the better choice as long as we accept that physically, the young forest class has not developed the characteristics of the forest class.

With this threshold, the majority of the managed forest is correctly picked out in both data sets. The thin belt of woodland running east-west to the south of West Harling is also correctly identified, as was confirmed using the Ordnance Survey map of this area. Inside West Harling, the small misclassified patches of forest all lie within young stands. In addition, changes in the forest from 1992/3 to 1997 are apparent, with several clearcut areas and young plantations in 1997, which were forest in 1992/3.

From the basic concept of the algorithm, it is clear that classification errors will occur for two types of regions:

1) nonforest areas whose average variation is less than the selected threshold;
2) forest regions whose average variation exceeds the threshold.

Types of target giving rise to the first type of error include urban areas or buildings (e.g., farm buildings to the north of the forest area) and grassland (such as occurs along the river valley, which cuts into the northwest of the forest). Some correction for this type of error should be possible by using absolute values of the backscattering coefficient. As shown in Fig. 6, for older forest areas, $-13\ \text{dB} < \sigma^o < -8\ \text{dB}$. Urban areas tend to contain bright targets whose RCS lies above this range, while grassland often appears darker than forest. In fact, tests at West Harling indicated little gain from this refinement, although more extensive evaluation is needed.

The second type of error occurs for young forest, whose response is essentially that of the underlying soil, until the canopy is sufficiently dense to cause significant attenuation of the soil return. In terms of the physical content of the radar backscatter, young forests are therefore comparable to certain agricultural crops or low bushland and cannot be detected correctly by the ERS SAR. Hence, correction of this type of error may require information not available from the radar data.

IV. Assessment of the Methodology

Quantitative assessment of the performance of this approach is difficult, because the only information about areas outside the managed forest is provided by the Ordnance Survey map. We therefore have little information on the nonforest class and limited information on other woodland. Even within the forest, a field visit indicated the difficulty of knowing how to interpret the data provided by the forestry map. Another possible means of assessing the ERS results is by comparing them with classifications by optical sensors. To this end, we employed the Land Cover Map of Great Britain (LCMGB), which was based on Landsat TM data acquired between 1989 and 1991. After registration using ground control points and appropriate geometrical transformations, this data was suitable for comparison with the 1992/93 ERS classification shown as Fig. 10(c).

The LCMGB records 25 cover types, of which two (coniferous and deciduous/evergreen woodland) correspond directly to forest, while a third (scrub/orchard) would also be expected to contribute to the forest class. Fig. 11(a) shows the results at West Harling of treating these as a single class, with all other cover types regarded as nonforest. The most obvious contrast with Fig. 10(c) comes from the large areas within the managed forest classified as nonforest. These are all young forest stands. Also noteworthy is the clear discrimination of the river and surrounding grassland penetrating into the northwest of the forest and the assignation of almost all the region outside the managed forest (with the exception of the narrow belt of woodland to the south) to the nonforest class.

The young forest areas are mainly assigned to two classes of the LCMGB: grass heath and meadow/ seminatural swards. Including these in the forest class leads to the result shown in Fig. 11(b). Two of the major holes in the managed forest area have been closed but at the expense of bringing the river valley and several of the agricultural areas into the forest class. The

Fig. 10. Mva images of West Harling derived from ERS-1 1992/3 and ERS-2 1997 data and classification results using different thresholds.

third main managed forest area identified as nonforest by TM (in fact classified as agricultural land) is just to the east of the river. This is a clear error, since the region consists entirely of Corsican pine planted in 1981. Apart from this, comparison with Fig. 10(c) indicates that the overall structure of the ERS and TM classifications are similar, although that for TM appears noisier. Around 67% of the pixels identified as forest by TM are similarly classified by ERS. The corresponding figure for nonforest is 73%. However, as we have seen, the TM results of Fig. 11(b) cannot be considered reliable and certainly provide no solid basis for assessing the ERS results.

A more general attempt to assess the above approach and compare it with forest estimates using other sensors was carried out within the EU Forest Monitoring in Europe using Remote Sensing (FMERS) Project [19]. The major emphasis of this study was on classification using a range of optical satellite data, but it included a SAR component based on ERS data.

The testsites for this project were selected to cover a range of forest types (coniferous, broad-leaved deciduous, broad-leaved evergreen, and mixed forest). A two-class separation into forest and nonforest was carried out using the ERS data by the method discussed in Section III. In some cases, the optical data considered just these two classes, while in other cases, separation into three or more classes was attempted. Geocoding issues meant that SAR/optical comparisons were only carried out at sites in the U.K. (Thetford), Finland, and Poland. Ground data for the performance assessment was based on transect information provided by independent investigators familiar with the local areas.

Table II shows SAR results for the U.K., Finnish, and Polish test sites. For the U.K. site, over 90% of the pixels along the transects were correctly classified, but this value needs to be qualified. The selected ground data transects ran only through the forest areas, so that the nonforest class was not properly represented. The correct way to interpret the value is that 10% of the forest pixels along the transects were misclassified (principally in the young plantation areas). However, the best optical result gave only 74% correct pixels in a three-class discrimination.

At the Finnish testsite, the principal cover types were boreal forest and water, with some agricultural areas and villages. Since water shows large dynamic range variations, depending on wind conditions, good classification performance (over 94%) is possible on this testsite. The best two class separations using

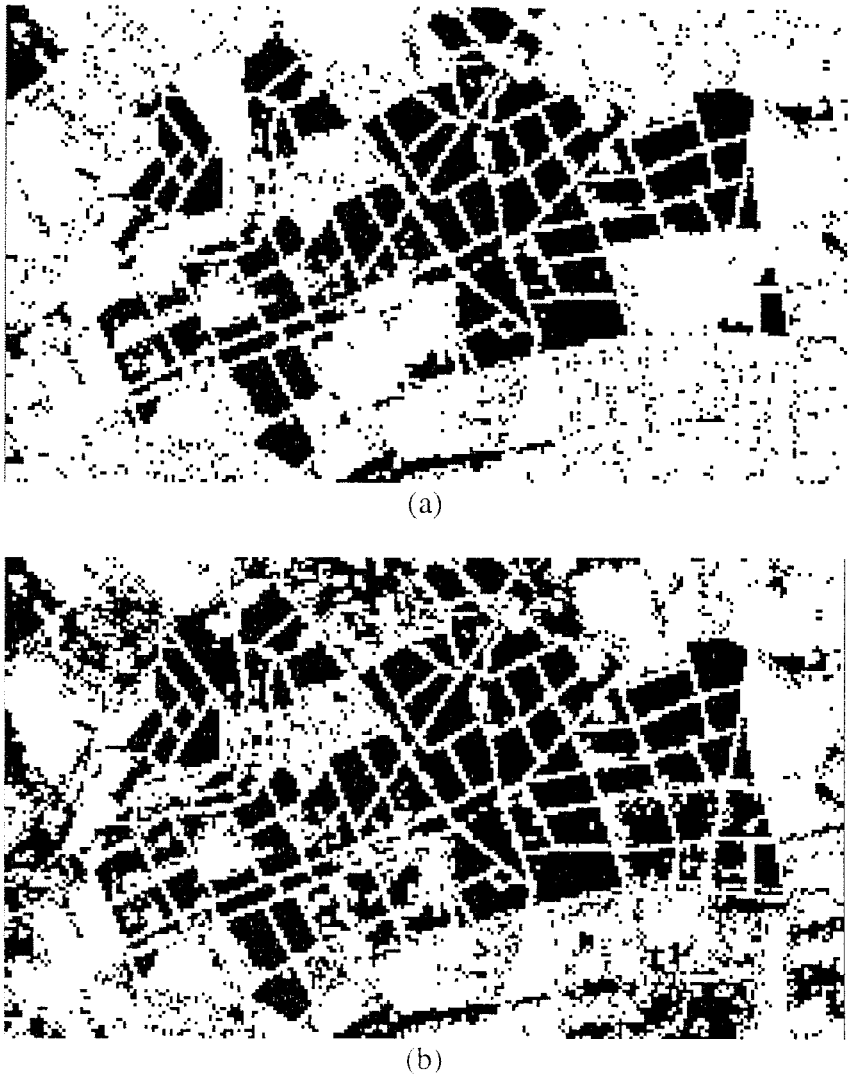

Fig. 11. (a) TM forest/nonforest classification overlaid with compartment boundaries. The forest class (black) contains three subclasses in the 25-class TM classification, namely scrub/orchard, deciduous woodland and coniferous/evergreen woodland and (b) As (a), but the forest class now includes two additional subclasses: grass heath and meadow/seminatural swards.

TABLE II
ERS SAR CLASSIFICATION RESULTS FOR THE FMERS TEST SITES

Site	No. of images	Season				
		Spr	Sum	Aut	Win	% correct
UK	11	✓	✓	✓	✓	90.7
Finland	15	✓	✓	✓	✓	94.1
	2		✓✓			90.4
Poland	2		✓		✓	77.4

optical data also gave 94% classification accuracy. It is noteworthy that while the best performance from the SAR uses all 15 available dates, over 90% correct classification is achieved when just two summer SAR images are used. At this time of the year, farming activity causes significant change in the agricultural areas, while the forest is stable. By contrast, classification accuracy drops to 84.6% when a winter–summer pair of images is used, because the presence of snow causes significant changes in both the forest and nonforest classes. The result at the Polish test site, although not as good as at the two other sites, is comparable to the result obtained with TM.

Note that the presence of relief prevented detailed geometric matching and hence evaluation by the transect method in the FMERS study. Relief also causes radiometric distortion, but the method developed for the SAR analysis should be resistant to such effects in moderate relief, because it relies on image ratios. However, it will have limitations in steep terrain because of layover, foreshortening, and the need for very precise registration.

V. DISCUSSION AND CONCLUSIONS

The only type of current satellite SAR data available for operational applications is C-band intensity data from ERS and

Radarsat. This state of affairs will continue into the Envisat and Radarsat-2 era, which makes it important to fully exploit the potential of this data type. This requires both understanding of where the relevant information is to be found in the data and appropriate methods to access it. Multitemporal signatures are particularly important in many applications. This paper has discussed a generic approach to multitemporal analysis and indicated how the approach can be matched to the problem of forest area measurement with ERS PRI data.

Observations and modelling suggest that the most telling discriminator of forest cover is temporal stability, as long as its biomass exceeds 30–40 tons/ha. This leads to a physically-based classification scheme with several attractive features:

- the methodology is physically-based and unsupervised;
- it is resistant to moderate relief and to systematic calibration errors;
- it appears robust, being applicable without modification at a wide range of test sites (although improved performance is possible if the change threshold is optimized to local conditions);
- it uses simple algorithms that have been optimized to the properties of ERS, but can be readily adapted to Radarsat (and other) data.

In addition, since the methodology is rule-based, its error sources (stable nonforest targets, forest regions exhibiting significant variability) are easy to identify but may not be easy to correct. Further work is needed on this issue.

Although not described in detail here, this approach has been compared with results using coherence data from a single ERS Tandem pair acquired during March 1997 [18]. It has been demonstrated elsewhere that thresholds on coherence can be used to discriminate forest and other cover types [20]. For the West Harling site, the coherence added no extra information on forest area and suffered from some confusion in the nonforest areas, probably due to working of agricultural fields in the day separating the Tandem pair of images. For King's Forest, the higher coherence of grassland allowed it to be much better discriminated from forest and removed the confusion in the temporal signature. However, coherence has similar problems to multitemporal analysis in detecting young forest, because coherence is significantly larger for young than for older forest (mainly because of the lack of attenuation of the high coherence signal from the ground). It is also relevant that interferometric data from the ERS pair of satellites is of limited availability, and new acquisitions will no longer be possible when ERS-1 is finally decommissioned.

An important operational issue not addressed here is the number of images needed for the mapping. For cost reasons, a tradeoff between the minimum number and the classification performance should be determined for a given site. Based on the temporal behavior of forest and nonforest classes, the best dates will be those that correspond to maximum changes in the nonforest classes in order to obtain the best contrast with the temporally stable forest classes. At Thetford, it has not proved easy to isolate a small number of images carrying all the essential change information, because of the complexity of the region. However, this is still being investigated, as a generally applicable methodological approach is needed. Certainly, one constraint on the use of temporal change for forest mapping in boreal (and probably alpine) regions is that times of freezing or snow need to be excluded, as these conditions cause marked changes in the forest backscatter. This is unlikely to be important in more temperate forests unless the frost is severe enough to reduce significantly the dielectric constant of the vegetation components.

The analysis above used the properties of the ERS data to derive a simplified filtering approach, but this can easily be modified to other datatypes. For JERS data, the much longer coherence times mean that the temporal filter would need to take account of correlation between images. This would also be true if the data sequence contained one or several Tandem pairs. However, the explicit form of the temporal filter given by (2) makes it easy to cater correctly for such cases. Note, in fact, that the filter (2) does not even require the datatypes to be the same and could be applied, for example, to combined ERS and JERS data, as long as they were accurately registered. The spatial filtering for such lower resolution data would still be simple because of the lack of texture. By contrast, the simple temporal filtering scheme is appropriate for fine mode Radarsat data, but the spatial filtering must take account of image texture.

Note that the FMERS study, in attempting to quantify classification performance, raised serious questions about the appropriate methodology for doing this. Access to area-extensive validated ground data on regions containing both forest and nonforest is not easily available but is crucial in any comprehensive assessment. Means to provide such data should form part of any attempt to apply these methods to large-scale problems. A deeper question raised by FMERS and the present study is in fact how we develop meaningful measures for forest mapping accuracy, since this depends on the definition of what constitutes forest land. For some purposes, this may depend on planned or potential use, rather than the current state of the land cover [21]. Our results, both for ERS and TM, indicate that areas that are labelled forest from the point of view of the forester can encompass a wide range of physical conditions to which remote sensing instruments are sensitive. Hence, under some conditions, misclassification may be more accurately described as incompatability of labelling systems. From the application point of view, the issue is to establish whether the labelling derived from remote sensing is stable in terms of the inferred parameters, and then to establish a link from the parameters to desired information. At core, the forestry components of this paper support the concept that C-band temporal change can provide a broad classification into biomass or an equivalent quantity. The step from this to a forest classification is not direct.

Although the data handling approach described in this paper has been developed in the context of forestry using ERS data, it is relevant to other data types and in applications for which the spatial structure of the scene remains essentially unchanged, and the information is contained in the multitemporal behavior of σ^0. Agriculture and hydrology provide two such examples. However, the details of the processing chain summarized in Fig. 8 need modification both for datatype differences [15] and the particular application.

ACKNOWLEDGMENT

The authors wish to thank M. Taylor of the U.K. Forestry Commission for help with ground and meteorological data at Thetford, U.K., and the European Space Agency for providing access to ERS data. They would like to extend our appreciation to the Institute of Terrestrial Ecology (ITE), Monks Wood, U.K., who supplied them with the LANDSAT TM land cover classes of West Harling and King's Forest from the ITE Land Cover Map of Great Britain. This data was supplied subject to a signed Data Licence Agreement between the Sheffield Centre for Earth Observation Science (SCEOS) and ITE.

REFERENCES

[1] T. Le Toan, A. Beaudoin, J. Riom, and D. Guyon, "Relating forest biomass to SAR data," *IEEE Trans. Geosci. Remote Sensing*, vol. 30, pp. 403–411, Mar. 1992.

[2] M. C. Dobson, F. T. Ulaby, T. Le Toan, A. Beaudoin, E. Kasischke, and N. L. Christensen, "Dependence of radar backscatter on coniferous biomass," *IEEE Trans. Geosci. Remote Sensing*, vol. 30, pp. 412–415, Mar. 1992.

[3] M. L. A. Imhoff, "Theoretical analysis of the effect of forest structure on Synthetic Aperture Radar backscatter and the remote sensing of forest biomass," *IEEE Trans. Geosci. Remote Sensing*, vol. 33, pp. 341–352, 1995.

[4] A. Beaudoin, T. Le Toan, S. Goze, E. Nezry, A. Lopes, E. Mougin, C. C. Hsu, H. C. Han, J. A. Kong, and R. T. Shin, "Retrieval of forest biomass from SAR data," *Int. J. Remote Sensing*, vol. 15, pp. 2777–2796, Mar. 1994.

[5] J. R. Baker, P. L. Mitchell, R. A. Cordey, G. B. Groom, J. J. Settle, and M. R. Stileman, "Relationship between physical characteristics and polarimetric radar backscatter for Corsican pine stands in Thetford Forest, U.K.," *Int. J. Remote Sensing*, vol. 15, pp. 2827–2849, 1994.

[6] C. C. Hsu, C. Han, R. T. Shin, J. A. Kong, A. Beaudoin, and T. Le Toan, "Radiative Transfer theory for polarimetric remote sensing of pine forest at P band," *Int. J. Remote Sensing*, vol. 15, pp. 2943–2954, 1994.

[7] S. Yueh, J. A. Kong, J. A. Jao, R. T. Shin, and T. Le Toan, "Branching model for vegetation," *IEEE Trans. Geosci. Remote Sensing*, vol. 30, pp. 390–402, Mar. 1992.

[8] G. Cookmartin, P. Saich, S. Quegan, R. Cordey, P. Burgess-Allen, and A. Sowter, "Using backscatter models to define the limits of crop information recovery from SAR data," in *Proc. 2nd Int. Workshop on Retrieval of Bio-Geophysical Parameters from SAR Data for Land Applications*, ESA SP-441, 1998, pp. 107–114.

[9] ESA Specialist Panel, *Satellite Radar in Agriculture*. Noordwijk, The Netherlands: European Space Agency, ESA SP-1185, 1995.

[10] J. B. Way, E. J. M. Rignot, K. C. McDonald, R. Oren, R. Kwok, G. Bonan, M. C. Dobson, L. A. Viereck, and J. E. Roth, "Evaluating the type and state of Alaska taiga forests with imaging radar for use in ecosystem models," *IEEE Trans. Geosci. Remote Sensing*, vol. 32, pp. 353–370, Mar. 1994.

[11] H. Laur, P. Bally, P. Meadows, J. Sanchez, B. Schaettler, and E. Lopinto, "Derivation of the backscattering coefficient σ^0 in ESA ERS SAR PRI products," *ESA Doc.:ES-TN-RS-PM-HL09*, no. 2, 1997.

[12] E. J. M. Rignot and J. J. van Zyl, "Change detection techniques for ERS-1 SAR data," *IEEE Trans. Geosci. Remote Sensing*, vol. 31, pp. 896–906, July 1993.

[13] C. J. Oliver and S. Quegan, *Understanding Synthetic Aperture Radar Images*. Norwood, MA: Artech House, 1998.

[14] J. Bruniquel and A. Lopes, "Multi-variate optimal speckle reduction in SAR imagery," *Int. J. Remote Sensing*, vol. 18, pp. 603–627, 1997.

[15] S. Quegan and T. Le Toan, "Analysing multitemporal SAR images," in *Proc. Segunda Jornada Latino Americana de Sensoriamento Remoto por Radar*, Santos, Brazil, Sept. 1998, pp. 17–25.

[16] A. Lopes, E. Nezry, R. Touzi, and H. Laur, "Structure detection and statistical adaptive speckle filtering in SAR images," *Int. J. Remote Sensing*, vol. 14, pp. 1735–1758, 1993.

[17] F. Ribbes, T. Le Toan, J. Bruniquel, N. Floury, N. Stussi, S. C. Liew, and U. R. Wasrin, "Deforestation monitoring in tropical regions using multitemporal ERS/JERS SAR and INSAR data," in *Proc. IGARSS'97*, vol. 4, 1997, pp. 1560–1562.

[18] S. Quegan, T. Le Toan, J. J. Yu, F. Ribbes, and N. Floury, "Estimating forest area with multitemporal ERS data," in *Proc. 2nd Int. Workshop on Retrieval of Bio-Geophysical Parameters from SAR Data for Land Applications*, Noordwijk, The Netherlands, 1998, pp. 277–284.

[19] T. Hame, *Final Report on Forest Monitoring in Europe with Remote Sensing (FMERS)*. Espoo, Finland: Centre for Earth Observation, 1999.

[20] U. Wegmuller and C. I. Werner, "Retrieval of vegetation parameters with SAR interferometry," *IEEE Trans. Geosci. Remote Sensing*, vol. 35, pp. 18–24, Jan. 1997.

[21] M. Kohl and R. Pavin, "Definition of a system of nomenclature for mapping European forests and for compiling a pan-European forest information system," in *EUR 16416 EN*. Brussels, Belgium: Office Official Pub. Eur. Communities, 1996, p. 238.

Shaun Quegan received the B.A. and M.Sc. degrees in mathematics in 1970 and 1972 from the University of Warwick, Warwick, U.K.. He received the Ph.D. degree in atmospheric modelling from the University of Sheffield, Sheffield, U.K., in 1982.

Between 1982 and 1986, he was a Research Scientist with the Marconi Research Centre, Chelmsford, U.K., and led the Remote Sensing Applications Group from 1984 to 1886. He established the SAR Research Group at the University of Sheffield in 1986, which led to his Professorship, awarded in 1993. In the same year, he helped to inaugurate the Sheffield Centre for Earth Observation Science, of which he remains the Director. He has broad interests in the physics, systems, and data analysis aspects of radar remote sensing, but more particularly in the exploitation of this technology in environmental science and land applications.

Thuy Le Toan received the Engineer degree and the Ph.D. degree in Nuclear Physics from the Paul Sabatier University, Toulouse, France **[Author: years?]** .

In 1973, she joined the Centre d'Etude Spatiale des Rayonnements **[Author: location?]**, where she led the Remote Sensing Group. Since 1973, her research activity has been in the area of microwave remote sensing applied to natural surfaces. Her research interests include experimentation and modeling of microwave interaction with agricultural and forested media and analysis of SAR images. Since January 1995, she has been with Centre d'Etudes Spatiales de la Biosphere (CESBIO), Toulouse, France, where she is presently one of the three group leaders and leader of the Radar Observation team. She has been a Project Coordinator and Principal Investigator on many European SAR campaigns over the last decade, and PI for several ERS-1, ERS-2, JERS-1, SIR-C/XSAR and RADARSAT projects. She has also been involved in numerous studies for the E.U., ESA, NASA, NASDA, and national organizations on the modelling of SAR data and the use of SAR in applications. These include coordination of the E.U. Framework 4 project: European Forestry Observations by Radars (EUFORA) and partnership in a CEO project on mapping the Siberian forests using radar (SIBERIA). She is Prime Contractor in the European Space Agency project on Soil Moisture Retrieval Algorithms using Active Remote Sensing and Partner in the ESA project on rice monitoring (RISAR).

Dr. Le Toan is a member the ASAR Science Advisory Group (ESA) and of the Electromagnetics Academy.

Jiong Jiong Yu was born in Shanghai, China. She received the First Class Honours degree in electrical and electronics engineering from the University of Sheffield, Sheffield, U.K., in 1996, where she is currently pursuing the Ph.D. degree.

She is currently a Research Assistant working on the EU project, SAR Imaging for Boreal Ecology and Radar Interferometry Application (SIBERIA). Previously, she has worked on the EU-funded European Forest Observations by Radars (EUFORA) and Forest Monitoring in Europe using remote rensing (FMERS) projects. Her particular interests are in the application of radar remote sensing to monitoring of forests.

Florence Ribbes received the Engineer degree and the M.S. degree in Spatial Techniques from the Ecole Superieure d'Agriculture de Purpan, Toulouse, France, in 1994, and 1995, respectively, and the Ph.D. degree in remote sensing from the Universite Paul Sabatier, Toulouse, France in 1998.

She is currently a Postdoctoral Fellow in radar remote sensing of vegetation at the Centre d'Etudes Spatiales de la Biosphere (CESBIO), Toulouse, France, which involves participation in several microwave remote sensing projects (ERS-1/2, JERS-1, Radarsat, INDREX, and RISAR). Her interests are in experimental analysis and radar image processing towards applications.

Nicolas Floury received the engineering degree in telecommunications from the Ecole Nationale Supérieure des Télécommunications, Paris, France, in 1993, and the Ph.D. degree in physics applied to remote sensing from Université Paris 7, Paris, France, in 1999.

His main interests are in electromagnetic modelling and signal processing applied to the study of the interaction between microwaves and natural surfaces.